Catalysis Today 160 (2011) 137–143

Contents lists available at ScienceDirect

Catalysis Today

journal homepage: www.elsevier.com/locate/cattod

Electronic structures of supported Pt and PtSn nanoparticles in the presence of adsorbates and during CO oxidation☆

Brian C. Vicente[a], Ryan C. Nelson[a], Jagdeep Singh[b], Susannah L. Scott[a,*], Jeroen A. van Bokhoven[b,c,**]

[a] Department of Chemical Engineering, University of California, Santa Barbara, CA, USA
[b] Institute for Chemical and Bioengineering, ETH Zurich, Switzerland
[c] Laboratory for Energy and the Environment, PSI, Switzerland

ARTICLE INFO

Article history:
Available online 1 September 2010

Keywords:
HERFD XANES
In situ spectroscopy
PtSn alloy
K-L zeolite
CO oxidation

ABSTRACT

The effect of support type and alloying with Sn on the electronic structure of supported Pt nanoparticles was investigated using in situ high energy resolution fluorescence-detected X-ray absorption near-edge spectroscopy (HERFD XANES) at the Pt L_3-edge. Pt and PtSn particles supported on K-L zeolite have similar electronic structures in the presence of individual adsorbates (H_2, O_2 or CO). Under CO, both types of nanoparticles undergo dispersion to small Pt carbonyl clusters stabilized by their interaction with basic oxygens in the zeolite pores. However, these two catalysts behave quite differently during CO oxidation under near-stoichiometric reaction conditions. The Pt in Pt/K-L remains oxidized, even at low temperatures, and displays much lower activity than Pt/Al_2O_3, whose particles are reduced and covered with adsorbed CO under the same reaction conditions. Alloying the Pt in Pt/K-L with Sn results in an electronic structure for Pt closer to that of Pt/Al_2O_3, which adsorbs CO preferentially at temperatures below ignition, while forming an oxide above ignition. The activity enhancement by Sn in PtSn/K-L makes it similar in activity to Pt/Al_2O_3.

1. Introduction

Supported Pt nanoparticles are used extensively as catalysts in the production of both petrochemicals and fine chemicals [1,2]. They are also a major component of the three-way catalysts used in catalytic converters for automobiles [3]. Enhancement of the catalytic activity or selectivity of supported Pt nanoparticles can be achieved through the deliberate choice of support [4–8], or the addition of a dopant or alloy metal [5,9,10]. Differences in the activities of these Pt-based catalysts arise due to changes in the electronic structure of the Pt valence shell, affecting the availability of the valence orbitals to form bonds with reactants during the catalytic cycle [11–13].

A vast number of studies have attempted to relate the activity of heterogeneous catalysts to their geometric and electronic structures. The majority of the work elucidating the electronic structure of supported Pt and bimetallic Pt-containing nanoparticles relies on IR spectroscopy of chemisorbed CO [5,14–23]. Changes in the C–O stretching frequency of linearly-adsorbed CO can be used to infer the effect of the support or dopant (alloy metal) on Pt. While this technique provides valuable insight into the electronic structure of supported Pt, it cannot be used to probe changes in the electronic structure of Pt in the presence of other (or no) adsorbates.

High energy X-ray absorption spectroscopy (XAS) is an element-specific technique that has been used to investigate the electronic structure of supported Pt nanoparticles [7,24–26]. XAS allows for direct probing of the Pt electronic structure in the presence of various adsorbates (or without any adsorbate), and the use of hard X-rays makes the technique viable under reaction conditions [24]. X-ray absorption near-edge spectroscopy (XANES) experiments involve the excitation of a core electron to the valence shell, and can be used to investigate the empty density-of-states (DOS) of the absorbing atom. Excitation at the Pt L_3-edge causes promotion of a $2p$ electron into the empty $5d$-DOS, probing the electronic structure of the Pt valence shell. The X-ray absorption process leads to a sharp feature at the absorption edge of the XAS spectrum, commonly called the whiteline. The intensity, shape and position of the whiteline provides information on both the geometric and electronic structure of the absorbing atom. High energy resolution fluorescence-detected X-ray absorption spectroscopy (HERFD XAS) is a technique in which XANES spectra are recorded with an instrumental broadening that is less than the core-hole lifetime

☆ This paper is for a special issue entitled "Heterogeneous Catalysis by Metals: New synthetic methods and characterization techniques for high reactivity" guest edited by Jinlong Gong and Robert Rioux.

* Corresponding author. Tel.: +1 805 893 5606; fax: +1 805 893 4731.
** Corresponding author at: Institute for Chemical and Bioengineering, ETH Zurich, Switzerland. Tel.: +41 446325542; fax: +41 446321162.
E-mail addresses: sscott@engineering.ucsb.edu (S.L. Scott), j.a.vanbokhoven@chem.ethz.ch (J.A. van Bokhoven).

0920-5861/$ – see front matter © 2010 Elsevier B.V. All rights reserved.
doi:10.1016/j.cattod.2010.07.017

broadening [27–30]. Selective detection of a single fluorescence decay channel results in a core-hole with a longer lifetime and thus less broadening. The features in a HERFD XANES spectrum are therefore sharper and better-resolved than in a conventional XANES spectrum.

Recently, we reported an XAS study of the electronic structure of monometallic and bimetallic Pt-containing nanoparticles supported on alumina in the presence of a variety of adsorbates [31]. In this contribution, the effect of the support on the electronic structure of monometallic Pt and bimetallic PtSn nanoparticles is explored under reaction conditions through the use of in situ HERFD XANES. We show how support-dependent changes in electronic structure influence activity for CO oxidation.

2. Materials and methods

2.1. Catalyst synthesis

Pt/Al_2O_3 (1.90 wt.% Pt) containing either small or large Pt particles was synthesized by the incipient-wetness method. 1.0 g $[Pt(NH_3)_4](NO_3)_2$ in 14 mL deionized water was added to 25 g γ-alumina (B.E.T. surface area, 180 m^2/g). After addition of an aqueous solution saturated with NH_4OH (2 mL), the mixture was dried overnight in air at 398 K. To obtain small or large Pt particles, the resulting powder was calcined for 3 h at 623 or 773 K, respectively. Both materials were reduced at 523 K in a flow of pure H_2 (100 mL/min). The Pt loading was determined by inductively-coupled plasma analysis.

PtSn particles supported on K-L zeolite (referred to below as K-L) were prepared by sequential impregnation of tin and platinum [9,10,32]. The incipient-wetness impregnation of Tosoh K-L (Si/Al = 6.2, 13.6 wt.% K), previously calcined in dry air at 873 K for 18 h, was performed using a solution of tributyltin acetate in methanol under a dry N_2 atmosphere. The Sn/K-L was dried in air and calcined at 573 K, followed by impregnation with an aqueous solution of $[Pt(NH_3)_4](NO_3)_2$ at room temperature. PtSn/K-L was dried at 573 K and reduced in H_2 at 873 K. The final catalyst contained 1.0 wt.% Pt and had a Pt:Sn ratio of 1.4:1. Pt/K-L was prepared similarly, omitting the addition of Sn.

2.2. Reactor setup

Catalytic combustion was conducted using a flow reactor described elsewhere [26]. The reactor, which resembles a plug-flow reactor with a diameter of 1.6 mm [33], was equipped with a transmission/fluorescence cell with aluminum windows to allow the simultaneous recording of XANES spectra. The temperature of the reactor was monitored by a thermocouple embedded in the reactor housing. The reactor was loaded with approx. 40 mg catalyst that had been sieved to obtain particle sizes in the range 65–125 μm. Gases were pre-mixed using computer-controlled mass-flow controllers. A computer-operated four-port valve was used for rapid switching between the adsorbing gases and helium. The outlet gases were monitored using a GSD Omnistar mass spectrometer from Pfeiffer Vacuum. Prior to XANES experiments, each catalyst was pre-treated in situ with 5 vol.% H_2 in He at 473 K, followed by pure He at 473 K for 30 min, then cooled in pure He to 303 K before switching to the desired adsorbing gas. XANES measurements were performed at a constant total flow rate of 30 mL/min, corresponding to a space velocity of ca. 64,000 h^{-1}.

CO oxidation was performed with a gas mixture containing 1% CO/1% O_2/He. A constant total flow rate of 30 mL/min was maintained during the reaction. The reactor was heated at a constant rate of 2 K/min until the temperature was 10 K above the ignition temperature. The reactor was then cooled to at least 40 K below the ignition temperature, and a second heating cycle to ignition was performed. Reported ignition temperatures correspond to the second heating cycle.

2.3. High energy resolution fluorescence-detected X-ray absorption spectroscopy

Measurements were performed on beamline ID 26 at the European Synchrotron Radiation Facility (ESRF) in Grenoble, France, using two u35 undulators. The X-ray beam incident on the sample measured 0.6 mm horizontally and 0.2 mm vertically. The incident energy, calibrated with a Pt foil, was selected by means of a pair of Si(1 1 1) crystals, with an energy bandwidth of 1.6 eV at the Pt L_3-edge. The total flux was 3×10^{13} photons/s. Higher harmonics were suppressed by two mirrors, one coated with Pd and the other with Cr, working at 3 mrad in total reflection.

High energy resolution emission detection was performed with a vertical-plane Rowland circle spectrometer tuned to the Pt $L_{\alpha 1}$ fluorescence line (9442 eV) and an avalanche photodiode for photon counting. A total energy bandwidth of 2.0 eV was achieved using the (6 6 0) Bragg reflection of four, spherically-bent Ge crystals (R = 1000 mm, d = 100 mm). This is below the lifetime broadening of the Pt $L_{\alpha 1}$ line, 2.2 eV, and is well below the $2p_{3/2}$ core-hole lifetime broadening of 5.3 eV [34]. A Canberra silicon photodiode was used to measure total fluorescence simultaneously with the HERFD XANES. Spectra were collected with a time resolution of 120 s at 303 K in pure He, 5% CO in He, 5% H_2 in He, and 5% O_2 in He. Spectra were collected continuously during the heating cycles of CO oxidation reactions in flowing 1% CO/1% O_2/He, as well as during in situ catalyst treatments (to ensure that unintended oxidation did not occur during cooling under He).

3. Results

3.1. Activity for CO oxidation

Fig. 1 shows the ignition curves recorded for CO oxidation over Pt/Al_2O_3, Pt/K-L, and PtSn/K-L. The differences among these catalysts in ignition temperature (the temperature at which CO conversion rises rapidly to completion) show that catalytic activity is influenced both by the alloying of Pt with Sn, and by the type of support. Pt/Al_2O_3 is the most active catalyst, with an ignition temperature of 477 K. Pt/K-L has substantially lower activity, with an ignition temperature of 511 K. However, when Pt is alloyed with a non-reactive metal, in this case Sn, the activity of the PtSn/K-L catalyst increases and becomes similar to that of Pt/Al_2O_3, with an ignition temperature of 478 K.

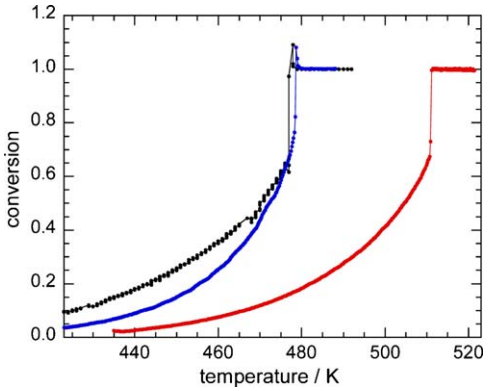

Fig. 1. Temperature dependence of the conversion of CO to CO_2 by 40 mg Pt/Al_2O_3 (black), Pt/K-L (red), or PtSn/K-L (blue), in flowing CO/O_2 (1% each in He, 30 mL/min). (For interpretation of the references to color in this figure legend, the reader is referred to the web version of the article.)

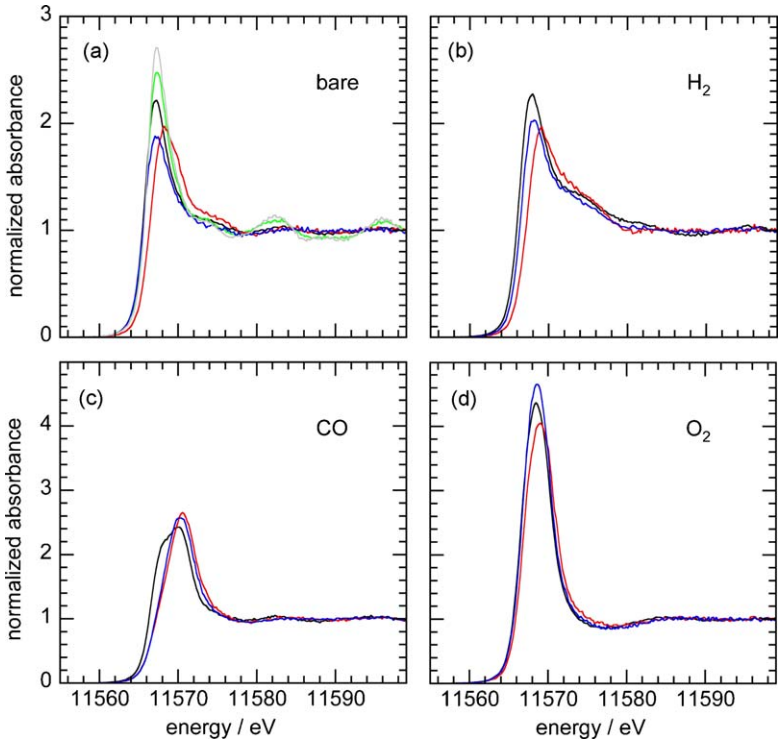

Fig. 2. Pt L_3-edge HERFD XANES for Pt/Al_2O_3 (small particles, black), Pt/Al_2O_3 (large particles, green), Pt/K-L (red), PtSn/K-L (blue), and Pt foil (grey), for (a) bare Pt; and (b) after H_2 adsorption, (c) after CO adsorption and (d) after O_2 adsorption, each at 303 K. (For interpretation of the references to color in this figure legend, the reader is referred to the web version of the article.)

3.2. Particle sizes of Pt and PtSn catalysts

Previous work has shown that Pt and PtSn nanoparticles, prepared in the same manner as the method used here and supported on γ-alumina, have average metal particle sizes below 1 nm [31]. Pt and PtSn nanoparticles supported on K-L are small enough to fit inside the zeolite cages without blocking the pores [35,36]. In order to confirm that the supported nanoparticles used in this study have comparable sizes, the multiple-scattering features in the HERFD XANES were examined. Fig. 2a shows the results for the supported Pt and PtSn catalysts as bare particles (i.e., no adsorbates), as well as the Pt foil. The multiple-scattering features at 11,582 and 11,596 eV are much more intense for the large Pt particles on γ-alumina and for the Pt foil than for the small particles in our Pt/Al_2O_3, Pt/K-L and PtSn/K-L catalysts. The much lower intensity of the multiple-scattering features at 11,582 and 11,596 eV in the spectra of the supported catalysts confirms that they all contain small Pt particles (presumably, ca. 1 nm diameter).

3.3. Effect of individual adsorbates on the electronic structures of Pt and PtSn catalysts

In order to probe differences in the electronic structures of the supported Pt and PtSn catalysts, HERFD XANES was recorded in the absence and presence of various adsorbates. Fig. 2 shows the results for Pt/Al_2O_3, Pt/K-L, and PtSn/K-L as (nominally) bare metal particles, as well as with adsorbed H_2, CO, and O_2. The whiteline energies and normalized intensities for all samples are reported in Tables 1 and 2, respectively.

In the absence of adsorbates, the spectrum of Pt/Al_2O_3 (small particles) shows a strong whiteline at 11,567.3 eV, corresponding to the $2p_{3/2}$-to-5*d* dipole transition. Pt/K-L and PtSn/K-L (bare metal particles) have whitelines at 11,568.4 and 11,567.3 eV, respectively. The whiteline intensity, which directly reflects the number of holes in the *d*-band [37–39], is higher for both Pt/Al_2O_3 samples than for either Pt or PtSn supported on K-L. The spectrum of Pt/K-L also shows additional intensity from 11,572 to 11,578 eV. It likely arises from the Pt–H antibonding states present upon adsorption of H_2 [40,41], and indicates that the H_2 used in the reduction step of catalyst preparation was incompletely removed from the Pt surface.

Upon adsorption of H_2, the whiteline intensity of Pt/Al_2O_3 does not change, however, its position shifts by 0.5 eV, to 11,567.8 eV. The whiteline of Pt/K-L, in which the particles were initially partly

Table 1
Energies (eV) of whiteline maxima for supported Pt nanoparticles in the presence of various adsorbates at 303 K.

Adsorbate	Pt/Al_2O_3	Pt/K-L	PtSn/K-L
None (bare particle)	11,567.3	11,568.4	11,567.3
H_2	11,567.8	11,569.0	11,568.1
CO	11,568.1	11,570.7	11,570.1
	11,570.1		
O_2	11,568.4	11,569.0	11,568.7
CO/O_2	11,568.4	11,569.0	11,569.5
	11,570.1		
Ignition[a]	11,567.8	11,569.2	11,568.1

[a] Recorded in flowing CO/O_2 at the ignition temperature.

Table 2
Maximum whiteline intensity in the normalized HERFD XANES of supported Pt nanoparticles in the presence of various adsorbates at 303 K.

Adsorbate	Pt/Al_2O_3	Pt/K-L	PtSn/K-L
None (bare particle)	2.21	1.97	1.87
H_2	2.28	2.03	1.95
CO	2.23	2.66	2.56
	2.41		
O_2	4.36	4.06	4.63
CO/O_2	2.18	3.62	2.75
	2.35		
Ignition[a]	3.26	4.87	3.46

[a] Recorded in flowing CO/O_2 at the ignition temperature.

covered by H_2, shows the same intensity upon exposure to flowing H_2 while shifting to 11,569.0 eV, corresponding to a 0.6 eV increase in energy. PtSn/K-L exhibits the largest shift in the position of its whiteline, moving 0.8 eV, to 11,568.1 eV, and experiences a slight increase in intensity. The spectra of the H_2-adsorbed materials also show increased intensity between 11,572 and 11,580 eV (even for Pt/K-L), which, as mentioned above, arises due to the newly-formed Pt–H antibonding states. Pt(large particles)/Al_2O_3 shows similar behavior to Pt(small particles)/Al_2O_3 in the presence of H_2 and with all other adsorbates (see below), although the adsorbate effects are less pronounced for the large particles due to the dominant contributions of non-surface Pt atoms (see Appendix A).

Adsorption of CO on Pt/K-L and PtSn/K-L results in whitelines with comparable intensities, located at 11,570.5 and 11,570.1 eV, respectively. Surprisingly, the doublet feature in the whiteline that is often observed for supported Pt particles covered with adsorbed CO is absent [25,26,30]. However, this doublet is observed in the spectrum of CO-exposed Pt/Al_2O_3, at 11,568.4 and 11,570.1 eV. Previous studies have shown that its low energy component arises from the Pt *d*-DOS, while the component at higher energy is the result of overlap between a CO antibonding orbital and a Pt *d*-orbital when CO is adsorbed in the atop configuration [25,30]. The higher energy component of the doublet appears at nearly the same energy as the whiteline in the spectra of the particles supported on K-L, suggesting that these materials contain CO adsorbed in a similar manner. However, the absence of the lower energy whiteline component for Pt/K-L and PtSn/K-L indicates that their structure under CO differs from that of Pt/Al_2O_3. EXAFS suggests that under CO, Pt/K-L is dispersed into smaller $Pt_3(CO)_n$ clusters that are stabilized within the pores of the zeolite [42]. This may explain the unique shape and position of the whiteline for the particles supported on K-L upon exposure to CO.

Although the electronic structures of Pt/K-L and PtSn/K-L appear to be rather similar in the presence of either H_2 or CO, differences in their whitelines are clearly evident when they are exposed to O_2. For PtSn/K-L, the whiteline position is 11,568.7 eV, similar to that for Pt/Al_2O_3, while for Pt/K-L it is shifted 0.3 eV higher, to 11,569.0 eV. The whiteline intensities are quite different for all three samples, with PtSn/K-L having the most intense whiteline, followed in order by Pt/Al_2O_3 and then Pt/K-L.

3.4. Electronic structure of catalysts under reaction conditions

HERFD XANES experiments were also conducted in situ, in order to probe the electronic structures of the catalysts during CO oxidation. Fig. 3 compares the HERFD XANES of the three catalysts at 303 K and at their ignition temperatures, in the presence of flowing 1% CO/1% O_2. At 303 K, the spectrum of Pt/Al_2O_3 is similar to that of Pt/Al_2O_3 with adsorbed CO, Fig. 2c. The doublet feature characteristic of CO adsorbed atop Pt is clearly evident. In the corresponding spectrum of PtSn/K-L, the whiteline is broader than when either CO or O_2 were adsorbed separately. Furthermore, the whiteline has a maximum intensity at 11,569.5 eV, which is intermediate between the positions of the whiteline when CO is adsorbed alone (11,570.1 eV) and when O_2 is adsorbed alone (11,568.7 eV). The electronic structure of Pt/K-L under the CO/O_2 mixture is apparently different from that of either of the other catalysts. The whiteline position, at 11,569.0 eV, is identical to that of Pt/K-L under O_2 alone. The whiteline intensity is also much higher than observed for the other two materials, resembling the spectrum of the O_2-exposed material. As with PtSn/K-L, the whiteline is broadened relative to the spectra recorded with individual adsorbates.

Upon heating each material to its ignition temperature in the presence of the CO/O_2 mixture, all three exhibit significant changes in their electronic structures. Once again, the spectra of Pt/Al_2O_3 and PtSn/K-L closely resemble one another, while the spectrum of Pt/K-L is clearly distinct. At ignition, the whiteline in the Pt/Al_2O_3 spectrum appears at 11,567.8 eV and no longer contains the high energy feature associated with CO adsorbed on Pt. The whiteline of PtSn/K-L is only 0.3 eV higher, at 11568.1 eV. Both spectra resemble those recorded under O_2 alone (Fig. 2d). The spectrum of Pt/K-L is substantially different, both in the intensity and the position of its whiteline. The position, 11,569.2 eV, is over 1.0 eV higher in energy than for either Pt/Al_2O_3 or PtSn/K-L, but the change in its position at ignition is only 0.2 eV relative to its position at 303 K. Furthermore, its intensity far exceeds that for the other samples, exceeding even that of Pt/K-L exposed only to O_2.

Fig. 4 shows the HERFD XANES spectra for the three catalysts under reaction conditions at temperatures below, at, and above ignition. The spectra highlight changes in electronic structures that occur upon reaching the ignition temperature. Pt/Al_2O_3 is converted from a CO-covered Pt(0) structure to a partially oxidized structure. The doublet characteristic of Pt with adsorbed CO is still observed just below ignition, although the relative intensities of the high and low energy components of the whiteline differ slightly from those in the spectrum collected at 303 K, since the low energy component is now more intense.

PtSn/K-L exhibits behavior similar to that of Pt/Al_2O_3, being converted from CO-covered Pt(0) to an oxide structure when the material is heated above its ignition temperature. Below ignition, the whiteline appears at 11,568.1 eV (i.e., the same as its position at ignition), but has a shoulder at higher energy due to residual adsorbed CO. The corresponding spectra for Pt/K-L show little difference below, at, and above its ignition temperature. A small increase in the intensity of the whiteline is the only change

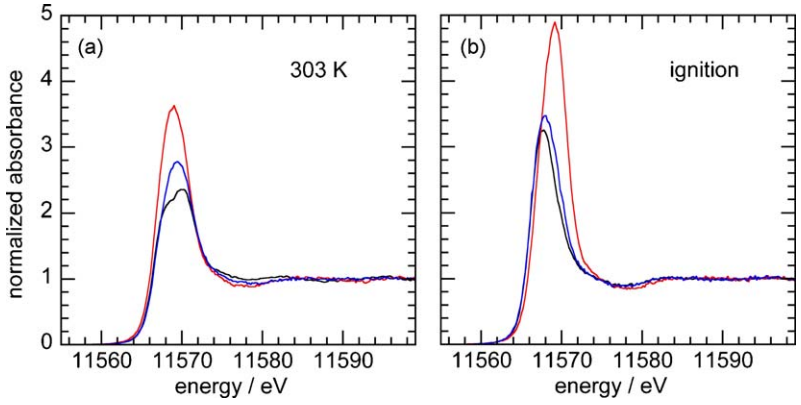

Fig. 3. Pt L_3-edge HERFD XANES for Pt/Al_2O_3 (black), Pt/K-L (red), and PtSn/K-L (blue), in a flowing stream of 1% CO/1% O_2 (balance He), at (a) 303 K; and (b) at their respective ignition temperatures. (For interpretation of the references to color in this figure legend, the reader is referred to the web version of the article.)

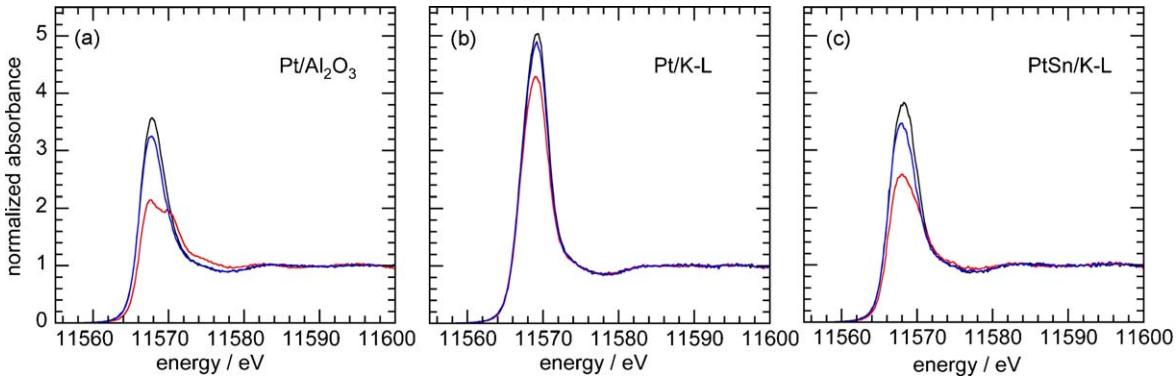

Fig. 4. Pt L_3-edge HERFD XANES for (a) Pt/Al_2O_3; (b) Pt/K-L; and (c) PtSn/K-L, in a flowing stream of 1% CO/1% O_2 (balance He) at 5 K below ignition (red), at ignition (blue), and at 5 K above ignition (black). (For interpretation of the references to color in this figure legend, the reader is referred to the web version of the article.)

observed as the temperature is raised. There is no evidence of adsorbed CO under any conditions. Instead, the partly oxidized Pt appears to be converted to an even more oxidized state.

4. Discussion

The ignition phenomenon observed during CO oxidation over Pt/Al_2O_3 is the result of a drastic structural change in the Pt particles, which HERFD XANES has proven capable of detecting [24]. CO oxidation over Pt is known to proceed via a Langmuir–Hinshelwood mechanism [43–45], in which both O_2 and CO must be adsorbed on the metal prior to reacting. At low temperatures, CO occupies most of the available adsorption sites and blocks the adsorption of O_2. As the temperature increases, less CO remains adsorbed on the Pt surface, exposing sites capable of the dissociative adsorption of O_2 [45]. When adsorbed oxygen is present, adsorbed CO is rapidly oxidized to CO_2, regenerating more vacant Pt sites. Below ignition, complete conversion is not achieved, and some CO remains strongly adsorbed on the Pt surface. When ignition is reached, this adsorbed CO is liberated and reacts, accounting for the transient observation of CO_2 generation at greater than 100% conversion. After this previously adsorbed CO reacts, a steady-state is achieved, with complete conversion of CO in the reactor feed.

While the conversion profiles of both Pt/Al_2O_3 and PtSn/K-L (Fig. 1) are consistent with this reaction mechanism, Pt/K-L appears to behave differently. Not only is its ignition temperature significantly higher, but excess CO_2 (beyond complete conversion) is not observed at ignition.

Although all three catalysts containing small particles show similar multiple-scattering features, the whitelines for both Pt/K-L and PtSn/K-L are less intense than the whiteline for Pt/Al_2O_3, Fig. 2a. This may indicate that the particles supported on K-L are slightly smaller than those supported on alumina. Smaller Pt particles have a lower average coordination number, less hybridization of the *s*, *p* and *d* valence orbitals, and fewer *d*-DOS above the Fermi level [46–49], resulting in decreased whiteline intensity. However, investigations of CO-covered Pt/K-L have suggested that basic oxygen sites in the zeolite can interact with the Pt particles, resulting in metal that is more electron-rich relative to Pt on other supports [35,50]. A similar effect could also explain the decreased intensity of the whitelines observed here for Pt/K-L and PtSn/K-L.

Alloying of Pt with Sn changes the ability of supported Pt particles on both alumina and K-L zeolite to chemisorb H_2 [10,31,36]. While the presence of Sn does not change the size of the metal particles on either support appreciably, it does dilute the surface Pt sites available for H_2 adsorption [5,14,15,51,52]. The HERFD XANES of Pt/K-L and PtSn/K-L with adsorbed H_2 both show increased intensity associated with Pt–H antibonding states between 11,572 and 11,578 eV, but the alloyed particles have less intensity in this region than the unalloyed particles, Fig. 2b. There is also a significant difference in the positions of the whitelines for Pt/K-L and PtSn/K-L, indicating that their electronic structures also differ, which may affect their ability to adsorb H_2.

These results demonstrate that the support exerts a strong influence on the electronic structure of the Pt particles when CO is adsorbed. For materials made with K-L, the position of the whiteline in the presence of CO is the same as the position of the high energy component of the doublet feature of Pt/Al_2O_3, indicating that overlap of the CO antibonding orbitals with the Pt *d*-DOS occurs in both Pt and PtSn supported on K-L. Electron donation from the K-L support to the Pt particles is expected to increase π-back-bonding from Pt to CO and, consequently, the Pt–CO bond strength. In a previous study of CO adsorbed on Pt/K-L, stabilization of Pt–CO clusters by basic framework oxygens was proposed [50].

EXAFS showed that exposure of Pt/K-L to CO results in the formation of Pt_3 clusters bearing several carbonyl ligands [42]. The anionic Chini complex $[Pt_3(CO)_6^{2-}]$ was observed when Pt supported on either zeolite X or Y was exposed to CO [53], although IR and EXAFS results suggest that the Pt carbonyl clusters formed on K-L are neutral [42,50]. Furthermore, the formation of the Chini complex on the zeolite supports is slow, requiring up to several days [53], which is much longer than the timescale of our HERFD XANES experiments. In contrast, neutral Pt carbonyl clusters form quickly in K-L upon exposure to CO [42,50]. The increased backbonding ability of the particles supported on K-L likely leads to the formation of smaller, neutral Pt clusters as the catalyst restructures in order to accommodate more Pt–CO bonds. The formation of neutral $Pt_x(CO)_y$ clusters with a much lower Pt–Pt coordination number than the original Pt particles may explain why the low energy component of the whiteline, which arises from the *d*-DOS of the Pt neighbors of the adsorbing atom, is not observed for Pt or PtSn supported on K-L.

The HERFD XANES of the three catalysts under flowing O_2 show some variation in whiteline intensity, although they all have similar whiteline positions. The higher intensity of the PtSn/K-L whiteline indicates that the Pt in this sample is more oxidized than in either Pt/K-L or Pt/Al_2O_3. The whiteline intensities of Pt/Al_2O_3 and PtSn/K-L are the highest for these materials under O_2, consistent with much of the Pt being oxidized under O_2 at 303 K. However, the whiteline of Pt/K-L is more intense under the CO/O_2 reaction mixture at ignition than under O_2 at 303 K. While electron donation by the support may stabilize a surface Pt oxide, the presence of CO may induce dispersion into smaller Pt clusters that can be more completely oxidized.

HERFD XANES collected in situ during CO oxidation allows for observation of the electronic states during catalysis, and can pro-

vide insight into the reaction mechanism. The in situ spectra show that Pt/Al_2O_3 and PtSn/K-L behave similarly during CO oxidation, and are consistent with the behavior of Pt nanoparticles on other supports [54]. Both show two features in their whitelines just below ignition, Fig. 4a and c. The high energy feature is due to adsorbed CO, while the low energy feature is likely due to oxidized Pt rather than the Pt *d*-DOS of reduced Pt. In addition, both become oxide-like upon heating to their ignition temperatures, Fig. 3b. Finally, both are oxidized further upon heating beyond the ignition temperature, Fig. 4. These results are consistent with the Langmuir–Hinshelwood reaction mechanism described above. Both catalysts have comparable reactivity for CO oxidation, as shown by their similar ignition temperatures.

Pt/K-L, which has a much higher ignition temperature than PtSn/K-L, does not show the same trends in its in situ HERFD XANES spectra during CO oxidation. At all temperatures under flowing CO/O_2, the spectrum of Pt/K-L resembles that of PtSn/K-L under O_2 alone. The whiteline intensity increases further upon heating. It appears that the Pt/K-L catalyst is partly oxidized (perhaps as a surface oxide) even at low temperatures, and is converted to a more fully oxidized structure as the temperature is raised. The HERFD XANES shows no evidence for CO adsorption on Pt/K-L during CO oxidation at any temperature. While electron donation from the K-L support is believed to make the Pt particles more susceptible to oxidation, this tendency is apparently suppressed by the presence of Sn, which may be oxidized preferentially over Pt.

The presence of cationic Sn in PtSn/K-L has been detected by Mössbauer spectroscopy, even after reduction in H_2 at 773 K [9]. TPR results confirmed that complete reduction of Sn in supported PtSn catalysts occurs only at temperatures above 873 K [55–58]. Since oxidized Sn is likely present under our reaction conditions, the electron-rich oxygens of the K-L support may interact with it rather than with Pt, and thereby decrease the susceptibility of Pt to oxidation. However, the preferential oxidation of Sn relative to Pt is not evident in the presence of a single adsorbate: Sn does not adsorb CO, while under O_2, both Sn and Pt are oxidized [59–63]. IR spectroscopy of CO adsorbed onto Pt/K-L and PtSn/K-L showed no difference in the υ(CO) frequencies of the two samples, demonstrating that Sn has a negligible effect on the electronic state of the Pt [58]. However, during CO oxidation, Sn participates in the dissociation of molecular oxygen, which can then react with CO adsorbed on the Pt [5,60,61]. Consequently, Pt/K-L and PtSn/K-L behave quite differently in the presence of the CO/O_2 mixture, despite their apparent similarity in the presence of H_2, CO, and O_2 individually.

5. Conclusions

The electronic structures of small Pt and PtSn nanoparticles supported on γ-alumina and K-L zeolite were investigated in the presence of individual adsorbates and under reaction conditions, via in situ HERFD XANES. Compared to Pt/Al_2O_3, the lower whiteline intensities of the bare particles in Pt/K-L and PtSn/K-L indicate that the zeolite-supported Pt particles are either smaller or more electron-rich as a result of electron donation from the zeolite support. Under CO, Pt and PtSn particles on K-L appear to disperse as $Pt_x(CO)_y$ clusters that are stabilized by their interaction with basic oxygen sites of the zeolite. While the electronic structures of Pt/K-L and PtSn/K-L appear similar in the presence of a single adsorbate, they differ significantly under reaction conditions. Like Pt/Al_2O_3, PtSn/K-L shows CO poisoning until its ignition temperature is reached, when a high-activity oxide structure is formed. However, for Pt/K-L, CO-covered Pt(0) is not observed under any reaction conditions. A partially oxidized Pt structure, possibly a surface oxide, is present at low temperatures until ignition is achieved, when further oxidation of Pt occurs.

Acknowledgements

The authors are grateful to ESRF, France, for beamtime at ID26, and to Dr. Pieter Glatzel for his assistance during the beamtime and helpful discussions. The authors would also like to thank Professor James Dumesic and Dr. Edward Kunkes for supplying the PtSn/K-L. Funding for this project was provided by the National Science Foundation (NSF) through the Center for New Technologies Through Catalysis (CENTC) as well as the International Research and Education in Engineering (IREE) Program (supplement to CBET 0854425), and by the Swiss National Science Foundation (SNF).

Appendix A. Supplementary data

Supplementary data associated with this article can be found, in the online version, at doi:10.1016/j.cattod.2010.07.017.

References

[1] G. Ertl, H. Knoezinger, F. Schueth, J. Weitkamp, Handbook of Heterogeneous Catalysis, Wiley-VCH, Weinheim, Germany, 2008.
[2] C.N. Satterfield, Heterogeneous Catalysis in Industrial Practice, 2nd ed., McGraw-Hill, New York, 1991.
[3] R.J. Farrauto, R.M. Heck, Catal. Today 51 (1999) 351.
[4] T. Visser, T.A. Nijhuis, A.M.J. Van der Eerden, K. Jenken, Y. Ji, W. Bras, S. Nikitenko, Y. Ikeda, M. Lepage, B.M. Weckhuysen, J. Phys. Chem. B 109 (2005) 3822.
[5] M.M. Schubert, M.J. Kahlich, G. Feldmeyer, M. Huttner, S. Hackenberg, H.A. Gasteiger, R.J. Behm, Phys. Chem. Chem. Phys. 3 (2001) 1123.
[6] B.L. Mojet, D.E. Ramaker, J.T. Miller, D.C. Koningsberger, Catal. Lett. 62 (1999) 15.
[7] B.J. McHugh, G. Larsen, G.L. Haller, J. Phys. Chem. 94 (1990) 8621.
[8] G. Larsen, G.L. Haller, Catal. Lett. 3 (1989) 103.
[9] R.D. Cortright, J.A. Dumesic, Appl. Catal. A 129 (1995) 101.
[10] R.D. Cortright, J.M. Hill, J.A. Dumesic, Catal. Today 55 (2000) 213.
[11] B. Hammer, J.K. Nørskov, Surf. Sci. 343 (1995) 211.
[12] B. Hammer, J.K. Nørskov, Nature 376 (1995) 238.
[13] T. Bligaard, J.K. Nørskov, S. Dahl, J. Matthiesen, C.H. Christensen, J. Sehested, J. Catal. 224 (2004) 206.
[14] M. Arenz, V. Stamenkovic, B.B. Blizanac, K.J. Mayrhofer, N.M. Markovic, P.N. Ross, J. Catal. 232 (2005) 402.
[15] V. Stamenkovic, M. Arenz, B.B. Blizanac, K.J.J. Mayrhofer, P.N. Ross, N.M. Markovic, Surf. Sci. 576 (2005) 145.
[16] S. Ozkara, A.E. Aksoylu, Appl. Catal. A 251 (2003) 75.
[17] R.K. Herz, A. Badlani, D.R. Schryer, B.T. Upchurch, J. Catal. 141 (1993) 219.
[18] A.G.T.M. Bastein, F.J.C.M. Toolenaar, V. Ponec, J. Catal. 90 (1984) 88.
[19] K. Balakrishnan, J. Schwank, J. Catal. 138 (1992) 491.
[20] G. Blyholder, J. Phys. Chem. 68 (1964) 2772.
[21] A. Palazov, K. Bonev, G. Kadinov, D. Shopov, G. Lietz, J. Voelter, J. Catal. 71 (1981) 1.
[22] G. Leclercq, L. Leclercq, R. Maurel, J. Catal. 50 (1977) 87.
[23] M.J. Kahlich, H.A. Gasteiger, R.J. Behm, J. Catal. 171 (1997) 93.
[24] J. Singh, E.M.C. Alayon, M. Tromp, O.V. Safonova, P. Glatzel, M. Nachtegaal, R. Frahm, J.A. van Bokhoven, Angew. Chem. Int. Ed. 47 (2008) 9260.
[25] P. Glatzel, J. Singh, K.O. Kvashnina, J.A. van Bokhoven, J. Am. Chem. Soc. 132 (2010) 2555.
[26] J. Singh, M. Tromp, O.V. Safonova, P. Glatzel, J.A. van Bokhoven, Catal. Today 145 (2009) 300.
[27] A. Nilsson, J. Hasselström, A. Föhlisch, O. Karis, L.G.M. Pettersson, M. Nyberg, L. Triguero, J. Electron Spectrosc. Relat. Phenom. 110–111 (2000) 15.
[28] T. Strunskus, O. Fuchs, L. Weinhardt, C. Heske, M. Guraya, M. Muhler, V. Staemmler, C. Wöll, J. Electron Spectrosc. Relat. Phenom. 134 (2004) 183.
[29] J.A. van Bokhoven, C. Louis, J.T. Miller, M. Tromp, O.V. Safonova, P. Glatzel, Angew. Chem. Int. Ed. 45 (2006) 4651.
[30] O.V. Safonova, M. Tromp, J.A. van Bokhoven, F.M.F. de Groot, J. Evans, P. Glatzel, J. Phys. Chem. B 110 (2006) 16162.
[31] J. Singh, R.C. Nelson, B.C. Vicente, S.L. Scott, J.A. van Bokhoven, Phys. Chem. Chem. Phys. 12 (2010) 5668.
[32] R.D. Cortright and J.A. Dumesic, U.S. Patent 5,736,478 (1998).
[33] N. Weiher, E. Bus, B. Gorzolnik, M. Moeller, R. Prins, J.A. van Bokhoven, J. Synchrotron Radiat. 12 (2005) 675.
[34] J.C. Fuggle, J.E. Inglesfield, Unoccupied Electronic States, Springer-Verlag, Berlin, 1992.
[35] A.Y. Stakheev, E.S. Shpiro, N.I. Jaeger, G. Schulz-Ekloff, Catal. Lett. 32 (1995) 147.
[36] S.J. Cho, R. Ryoo, Catal. Lett. 97 (2004) 71.
[37] F.W. Lytle, J. Catal. 43 (1976) 376.
[38] A.N. Mansour, J.W. Cook Jr., D.E. Sayers, J. Phys. Chem. 88 (1984) 2330.
[39] D. Bazin, D. Sayers, J.J. Rehr, C. Mottet, J. Phys. Chem. B 101 (1997) 5332.
[40] D.C. Koningsberger, D.E. Ramaker, J.T. Miller, J. De Graaf, B.L. Mojet, Top. Catal. 15 (2001) 35.

[41] D.C. Koningsberger, M.K. Oudenhuijzen, J.H. Bitter, D.E. Ramaker, Top. Catal. 10 (2000) 167.
[42] B.L. Mojet, J.T. Miller, D.C. Koningsberger, J. Phys. Chem. B 103 (1999) 2724.
[43] T. Engel, G. Ertl, Adv. Catal. 28 (1979) 1.
[44] G. Ertl, Adv. Catal. 37 (1990) 213.
[45] P.D. Nolan, B.R. Lutz, P.L. Tanaka, J.E. Davis, C.B. Mullins, J. Phys. Chem. 111 (1999) 3696.
[46] L.F. Mattheiss, R.E. Dietz, Phys. Rev. B: Condens. Matter Mater. Phys. 22 (1980) 1663.
[47] M.G. Mason, Phys. Rev. B: Condens. Matter Mater. Phys. 27 (1983) 748.
[48] H. Häkkinen, M. Moseler, U. Landman, Phys. Rev. Lett. 89 (2002) 033401.
[49] P.K. Jain, Struct. Chem. 16 (2005) 421.
[50] A.Y. Stakheev, E.S. Shpiro, N.I. Jaeger, G. Schulz-Ekloff, Catal. Lett. 34 (1995) 293.
[51] D.A. Asbury, G.B. Hoflund, Surf. Sci. 199 (1988) 552.
[52] R. Bouwman, L.H. Toneman, A.A. Holscher, Surf. Sci. 35 (1973) 8.
[53] G. Schulz-Ekloff, R.J. Lipski, N.I. Jaeger, P. Huelstede, L. Kubelkova, Catal. Lett. 30 (1995) 65.
[54] E.M.C. Alayon, J. Singh, M. Nachtegaal, M. Harfouche, J.A. van Bokhoven, J. Catal. 263 (2009) 228.
[55] S. Zhang, Y. Zhou, Y. Zhang, L. Huang, Catal. Lett. 135 (2010) 76.
[56] L. Bai, Y. Zhou, Y. Zhang, H. Liu, M. Tang, Catal. Lett. 129 (2009) 449.
[57] A.D. Ballarini, C.G. Ricci, S.R. de Miguel, O.A. Scelza, Catal. Today 133–135 (2008) 28.
[58] J.H. Chae, S.H. Moon, Stud. Surf. Sci. Catal. 105B (1997) 877.
[59] G.C. Bond, Heterogeneous Catalysis, Oxford University Press (Clarendon), London, 1987.
[60] G.B. Hoflund, D.A. Asbury, P. Kirszensztejn, H.A. Laitinen, Surf. Interface Anal. 9 (1986) 169.
[61] C. Dupont, Y. Jugnet, D. Loffreda, J. Am. Chem. Soc. 128 (2006) 9129.
[62] P. Liu, A. Logadottir, J.K. Nørskov, Electrochim. Acta 48 (2003) 3731.
[63] T.E. Shubina, M.T.M. Koper, Electrochim. Acta 47 (2002) 3621.